Inorganic Chemistry

Article

pubs.acs.org/IC

Synthesis, Structure, and Physical Properties of $Ln(Cu,Al,Ga)_{13-x}$ (Ln = La−Pr, and Eu) and $Eu(Cu,Al)_{13-x}$

W. Adam Phelan,[†] Michael J. Kangas,[†] Gregory T. McCandless,[†] Brenton L. Drake,[†] Neel Haldolaarachchige,[‡] Liang L. Zhao,[§] Jiakui K. Wang,[§] Xiaoping P. Wang,[∥] David P. Young,[‡] Emilia Morosan,[§] Christina Hoffmann,[∥] and Julia Y. Chan*,[†]

[†]Department of Chemistry and [‡]Department of Physics and Astronomy, Louisiana State University, Baton Rouge, Louisiana 70803, United States

[§]Department of Physics and Astronomy, Rice University, Houston, Texas 77005, United States

[∥]Chemical and Engineering Materials Division, Neutron Sciences Directorate, Oak Ridge National Laboratory, Tennessee 39831, United States

Supporting Information

ABSTRACT: $Ln(Cu,Al,Ga)_{13-x}$ (Ln = La−Pr, and Eu; $x \sim 0.2$) were synthesized by a combined Al/Ga flux. Single crystal X-ray and neutron diffraction experiments revealed that these compounds crystallize in the $NaZn_{13}$ structure-type (space group $Fm\bar{3}c$) with lattice parameters of $a \sim 12$ Å, $V \sim 1600$ Å, and $Z \sim 8$. Our final neutron models led us to conclude that Cu is occupationally disordered on the 8*b* Wyckoff site while Cu, Al, and Ga are substitutionally disordered on the 96*i* Wyckoff site of this well-known structure-type. The magnetic susceptibility data show that $Ce(Cu,Al,Ga)_{13-x}$ and $Pr(Cu,Al,Ga)_{13-x}$ exhibit paramagnetic behavior down to the lowest temperatures measured while $Eu(Cu,Al,Ga)_{13-x}$ displays ferromagnetic behavior below 6 K. $Eu(Cu,Al)_{13-x}$ was prepared via arc-melting and orders ferromagnetically below 8 K. The magnetocaloric properties of $Eu(Cu,Al,Ga)_{13-x}$ and $Eu(Cu,Al)_{13-x}$ were measured and compared. Additionally, an enhanced value of the Sommerfeld coefficient (γ = 356 mJ/mol-K^2) was determined for $Pr(Cu,Al,Ga)_{13-x}$. Herein, we present the synthesis, structural refinement details, and physical properties of $Ln(Cu,Al,Ga)_{13-x}$ (Ln = La−Pr, and Eu) and $Eu(Cu,Al)_{13-x}$.

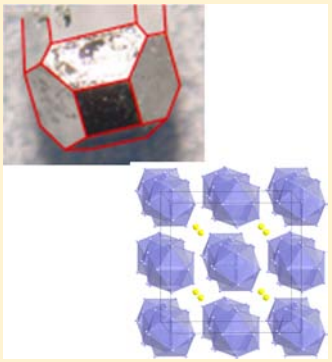

INTRODUCTION

Lanthanide intermetallic compounds adopting the $NaZn_{13}$ structure-type display highly correlated electron behavior and are of great interest to solid state physicists and chemists. Of particular interest is the valence instability of 4*f* and 5*f* electrons in Ce-, Yb-, or U-based compounds which leads to Kondo and heavy-fermion behavior, and several classes of these materials have been reviewed.[1−6] Heavy-fermion compounds exhibit an anomalously large electronic contribution to the heat capacity $C_p = \gamma T + \beta T^3$, with γ typically greater than 200 mJ/mol-K^2. UBe_{13} was reported to be a heavy-fermion defined by its anomalously large electronic specific-heat coefficient $\gamma \sim 1100$ mJ/mol-K^2 at low temperatures and shows an unconventional superconducting state mediated by the *f*-electrons below 0.85 K.[7−11] Enhanced mass ($\gamma \sim 58$ mJ/mol-K^2) has also been reported for $CeBe_{13}$ which is a mixed valence system (Ce^{4+}/Ce^{3+}).[10,12,13]

Although there are several examples of Ce-, Yb-, and U-based heavy-fermion systems, examples of Pr based heavy-fermion systems are more limited. The Heusler-type $PrInAg_2$ ($\gamma \sim 6500$ mJ/mol-K^2) has been reported as the first Pr-based heavy-fermion compound.[14] We have also reported that $Pr(Cu,Ga)_{13-x}$ shows heavy-fermion behavior with $\gamma \sim 100$ mJ/mol-K^2 and it follows the expected Kadowaki−Woods relations, $A/\gamma^2 \sim 1 \times 10^{-5}$ μ Ω-cm (mol-K/mJ^2),[15−17] where A is the coefficient of the quadratic term in the temperature dependent resistivity.

In light of the discovery of an enhanced mass state in $Pr(Cu,Ga)_{13-x}$, it was of interest to explore how substitution of Ga with Al would impact the structure and physical properties. Early attempts by our group to grow $Pr(Cu,Al)_{13-x}$ single crystals using the flux-growth procedure were unsuccessful. Perhaps the structurally related $Ln(Cu,Al)_{12}$ phases which crystallize in $ThMn_{12}$ structure-type are more robust as we have shown that the $Ln(Cu,Al)_{12}$ (Ln = Y, Ce−Nd, Sm, Gd−Ho and Yb) compounds can be prepared via an Al flux.[18] However, $Ln(Cu,Al)_{13}$ (Ln = La−Nd, Sm, and Eu) have been prepared via arc-melting, thus suggesting that more extreme synthetic conditions are needed to yield the $Ln(Cu,Al)_{13}$ (Ln = early lanthanide) phases.[19−22] The addition of Ga into the reactant mixture led to the crystallization of large (>5 × 5 × 5 mm^3) cubes of $Ln(Cu,Al,Ga)_{13-x}$ (Ln = La−Pr, and Eu). Attempts to prepare these phases using latter lanthanides resulted in phases which adopted the $ThMn_{12}$ structure-type. This is consistent with our previous findings where it was observed that Ga flux

Received: May 18, 2012
Published: September 10, 2012

   dx.doi.org/10.1021/ic301024t | *Inorg. Chem.* 2012, 51, 10193−10202

Table 1. Crystallographic Parameters for $Ln(Cu,Al,Ga)_{13-x}$ (Ln = La−Pr, and Eu) Obtained from Neutron Diffraction

	$La(Cu,Al,Ga)_{13-x}$	$Ce(Cu,Al,Ga)_{13-x}$	$Pr(Cu,Al,Ga)_{13-x}$	$Eu(Cu,Al,Ga)_{13-x}$
refined formula	$LaCu_{6.33}Al_{4.53}Ga_{1.97}$	$CeCu_{6.62}Al_{3.95}Ga_{2.28}$	$PrCu_{6.04}Al_{3.02}Ga_{3.84}$	$EuCu_{5.87}Al_{4.42}Ga_{2.48}$
formula weight (g/mol)	800.51	826.18	873.81	816.95
space group	$Fm\bar{3}c$	$Fm\bar{3}c$	$Fm\bar{3}c$	$Fm\bar{3}c$
crystal system	cubic	cubic	cubic	cubic
a (Å)	11.897(4)	11.863(3)	11.858(4)	11.921(3)
V (Å^3)	1683.7(10)	1669.3(8)	1667.4(9)	1694.2(8)
Z	8	8	8	8
T (K)	296(2)	296(2)	296(2)	296(2)
collected reflections	1949	2982	2322	2103
crystal size (mm^3)	0.76 × 2.10 × 2.75	1.80 × 2.10 × 2.70	1.12 × 2.36 × 2.86	1.44 × 1.82 × 2.06
S	1.08	1.06	1.08	1.03
$R_1[F^2 > 2\sigma(F^2)]^a$	0.057	0.050	0.051	0.077
$wR_2(F^2)^b$	0.156	0.143	0.140	0.194
$\Delta\rho_{max}$ (fm Å^{-3})	1.60	1.12	1.30	1.93
$\Delta\rho_{min}$ (fm Å^{-3})	−1.30	−1.08	−1.35	−1.14

$^a R_1(F) = \sum||F_o| - |F_c||/\sum|F_o|$. $^b wR_2(F^2) = [\sum[w(F_o^2 - F_c^2)^2]/\sum[w(F_o^2)^2]]^{1/2}$; $w = 1/[\sigma^2(F_o^2) + (0.105P)^2 + 37.065P]$, $w = 1/[\sigma^2(F_o^2) + (0.1072P)^2 + 9.9351P]$, $w = 1/[\sigma^2(F_o^2) + (0.1032P)^2 + 12.7889P]$, and $w = 1/[\sigma^2(F_o^2) + (0.1557P)^2 + 59.56P]$ for $La(Cu,Al,Ga)_{13-x}$, $Ce(Cu,Al,Ga)_{13-x}$, $Pr(Cu,Al,Ga)_{13-x}$, and $Eu(Cu,Al,Ga)_{13-x}$, respectively.

growth led to the formation of $Ln(Cu,Ga)_{13-x}$ (Ln = La−Nd and Eu)[16] and $Ln(Cu,Ga)_{12}$ (Ln = Y, Gd−Er, Yb),[18] thus suggesting that these phases which adopt the $NaZn_{13}$ and $ThMn_{12}$ structure-types are stable for early and late lanthanides, respectively.

In addition to exploring the enhanced mass behavior in these classes of materials, we have explored the magnetocaloric properties of certain members of this class of materials. Specifically, a polycrystalline sample of $Eu(Cu,Al)_{13-x}$ was prepared to compare its magnetocaloric properties to those of $Eu(Cu,Al,Ga)_{13-x}$. A polycrystalline sample was prepared because much like $Pr(Cu,Al)_{13-x}$, single crystals of $Eu(Cu,Al)_{13-x}$ could not be grown. Herein, the structures as determined from neutron and X-ray diffraction (XRD) and the physical properties of $Ln(Cu,Al,Ga)_{13-x}$ (Ln = La−Pr, and Eu) and $Eu(Cu,Al)_{13-x}$ are presented.

EXPERIMENTAL SECTION

Synthesis. Single crystals of $Ln(Cu,Al,Ga)_{13-x}$ (Ln = La−Pr and Eu) were synthesized via the flux-growth method. Ln = La−Pr, and Eu (99.9% purity), Cu (99.999% purity), Al (99.999% purity), and Ga (99.9999% purity) were placed into 2-mL alumina crucibles in a 1:9:10:10 molar ratio of Ln: Cu: Al: Ga. These filled alumina crucibles were then vacuum-sealed into separate fused silica tubes and placed into a furnace. These reaction ampules were heated at a rate of 200 °C/h to a maximum dwell temperature of 1100 °C. The ampules were allowed to dwell at this temperature for 10 h before being cooled to 480 °C at a rate of 2 °C/h. The excess molten flux was then separated from cubic single crystals via centrifugation. A dilute HNO_3 solution was used to chemically etch any remaining flux on the surface of the crystals. The crystals were observed to be slightly air and moisture sensitive over a period of months.

To prepare $Eu(Cu,Al)_{13-x}$, we used a similar strategy employed by Nordell and Miller.[23] A polycrystalline button of $Eu(Cu,Al)_{13-x}$ was prepared by arc-melting Eu, Cu, and Al in a 1:6.5:6.5 molar ratio in a water-cooled copper hearth under the flow of ultrahigh-purity argon gas inside a purged vacuum chamber. A Zr "oxygen getter" button was melted prior to arc-melting the elements to produce the compound. The $Eu(Cu,Al)_{13-x}$ button was turned over repeatedly and remelted several times to ensure homogeneity. The resulting mass loss of this button was negligible. The arc-melted button was sealed into an evacuated silica tube and then placed into a furnace where it was allowed to anneal for five days at 500 °C.

Single-Crystal XRD. Single crystals of $Ln(Cu,Al,Ga)_{13-x}$ (Ln = La−Pr and Eu) were mounted onto separate glass fiber tips using epoxy, attached to a goniometer head, and placed on a Nonius KappaCCD X-ray diffractometer equipped with Mo Kα radiation (λ = 0.71073 Å). The crystallographic parameters obtained from room temperature data collections for all compounds are provided in the Supporting Information, Table S1. The cubic Laue symmetry $m\bar{3}m$ and systematic absences led to the space group selection of $Fm\bar{3}c$ (No. 226). The generation of the initial model and subsequent structure refinement were conducted using SIR97 and SHELXL97, respectively.[24,25] All models were corrected for extinction (SHELXL method) as well as absorption (multi-scan method).[26] After locating all the atomic positions, the displacement parameters were refined anisotropically and weighting schemes were applied during the final stages of refinement. The atomic coordinates, site occupancies, and the displacement parameters determined for these compounds are listed in Supporting Information, Table S2. Selected interatomic distances for all analogues are provided in Supporting Information, Table S3.

Elemental Analysis. The elemental compositions of single crystals of $Ln(Cu,Al,Ga)_{13-x}$ (Ln = La−Pr and Eu) were analyzed using a Hitachi S-3600N scanning electron microscope (SEM) equipped with an energy dispersive spectroscopy (EDS) option. An average of six scans with 60 s counting times were performed on the clean, freshly exposed surfaces of cleaved and, etched single crystals with an accelerating voltage of 15 keV and a beam-to-sample distance of 20 mm. The compositions determined for each analogue from these elemental experiments when normalized by the at % Ln were found to have approximate composition of $La_{1.0}Cu_{6.3(6)}Al_{4.2(8)}Ga_{2.1(1)}$, $Ce_{1.0}Cu_{6.6(2)}Al_{4.4(5)}Ga_{1.9(1)}$, $Pr_{1.0}Cu_{6.0(3)}Al_{4.3(4)}Ga_{2.0(1)}$, and $Eu_{1.0}Cu_{5.9(3)}Al_{5.2(5)}Ga_{1.7(1)}$.

Single Crystal Neutron Diffraction. Single crystal neutron diffraction experiments were performed using the TOPAZ beamline at the Spallation Neutron Source at Oak Ridge National Laboratory.[27,28] Single crystals with dimensions of ∼4 mm^3 were mounted onto a vanadium post with glue and positioned onto the goniometer. Data collections were conducted at room temperature in wavelength-resolved time-of-flight (TOF) Laue mode using neutrons with wavelengths in the range of 0.6 to 3.5 Å. To ensure good coverage and redundancy for each data collection, data were collected with 14 detectors and using 10−16 crystals orientations, which were selected by evaluation with CrystalPlan software,[29] with collection times of approximately 2 h per orientation. Data were corrected for background and detector efficiency. Data reduction including neutron TOF spectrum and absorption corrections for all analogues were carried out with the ANVRED2 program of the ISAW program suite.[30] The reduced data were saved in SHELX HKLF2 format in which the

dx.doi.org/10.1021/ic301024t | Inorg. Chem. 2012, 51, 10193−10202

Table 2. Atomic Fractional Coordinates, Site Occupancies, and U_{eqs} for $Ln(Cu,Al,Ga)_{13-x}$ (Ln = La−Pr, and Eu) Obtained from Neutron Diffraction

atom	Wyckoff Site	x	y	z	occupancy	U_{eq} (Å^2)[a]
La1	8*a*	$^1/_4$	$^1/_4$	$^1/_4$	1	0.0062(2)
Cu1 (M1)	8*b*	0	0	0	0.828(10)	0.0077(3)
Cu2 (M2)	96*i*	0.11918(3)	0.17745(3)	0	0.4585(12)	0.01071(12)
Al2 (M2)	96*i*	0.11918(3)	0.17745(3)	0	0.38(2)	0.01071(12)
Ga2 (M2)	96*i*	0.11918(3)	0.17745(3)	0	0.164(16)	0.01071(12)
Ce1	8*a*	$^1/_4$	$^1/_4$	$^1/_4$	1	0.0061(3)
Cu1 (M1)	8*b*	0	0	0	0.851(9)	0.0086(2)
Cu2 (M2)	96*i*	0.11924(2)	0.17755(2)	0	0.4808(11)	0.01123(9)
Al2 (M2)	96*i*	0.11924(2)	0.17755(2)	0	0.33(2)	0.01123(9)
Ga2 (M2)	96*i*	0.11924(2)	0.17755(2)	0	0.1980(18)	0.01123(9)
Pr1	8*a*	$^1/_4$	$^1/_4$	$^1/_4$	1	0.0059(3)
Cu1 (M1)	8*b*	0	0	0	0.899(11)	0.0086(2)
Cu2 (M2)	96*i*	0.11929(2)	0.17765(2)	0	0.4284(13)	0.01109(10)
Al2 (M2)	96*i*	0.11929(2)	0.17765(2)	0	0.252(18)	0.01109(10)
Ga2 (M2)	96*i*	0.11929(2)	0.17765(2)	0	0.320(19)	0.01109(10)
Eu1	8*a*	$^1/_4$	$^1/_4$	$^1/_4$	1	0.0090(4)
Cu1 (M1)	8*b*	0	0	0	0.767(17)	0.0085(5)
Cu2 (M2)	96*i*	0.11855(5)	0.17745(4)	0	0.4252(16)	0.01180(17)
Al2 (M2)	96*i*	0.11855(5)	0.17745(4)	0	0.37(3)	0.01180(17)
Ga2 (M2)	96*i*	0.11855(5)	0.17745(4)	0	0.21(3)	0.01180(17)

[a] U_{eq} is defined as one-third of the trace of the orthogonalized U_{ij} tensor.

Table 3. Selected Interatomic Distances (Å) for $Ln(Cu,Al,Ga)_{13-x}$ (Ln = La−Pr, and Eu) Obtained from Neutron Diffraction

bonds[a]	La(Cu,Al,Ga)$_{13-x}$	Ce(Cu,Al,Ga)$_{13-x}$	Pr(Cu,Al,Ga)$_{13-x}$	Eu(Cu,Al,Ga)$_{13-x}$
Ln1−M2	3.4659(12)	3.4554(10)	3.4535(11)	3.4765(10)
M1−M2	2.5430(9)	2.5371(8)	2.5375(8)	2.5441(9)
M2−M2	2.5167(10)	2.5079(8)	2.5053(9)	2.5313(11)
M2−M2	2.6358(10)	2.6297(8)	2.6302(9)	2.6393(10)

[a] M1 = Cu1; M2 = Cu2, Al2, and Ga2.

wavelength is recorded separately for each individual reflection, and the reduced data were not merged as consequence of this saved format. Initial models were based on the single crystal XRD refinement results, and the neutron models were refined using SHELXL97.[25] Restraints on the elemental compositions were applied in accordance with the elemental analysis results, and extinction corrections were refined for each model. During the final stages of refinement, all atoms were modeled anisotropically and weighting schemes were applied. Details regarding data collections and refinements are given Table 1, atomic positions with site occupancies and U_{eqs} are given in Table 2, and bond distances are listed in Table 3. Because of the systematic similarites of analogues presented in this manuscript, only the structural models for La(Cu,Al,Ga)$_{13-x}$ will be described in detail in the Results and Discussion section.

Powder XRD. Portions of the annealed Eu(Cu,Al)$_{13-x}$ button were ground up using a mortar and pestle. A powder XRD pattern was obtained using a Bruker AXS D8 Advance diffractometer equipped with a Cu Kα_1 radiation source (λ = 1.54056 Å). To enhance the signal-to-noise ratio and obtain a higher resolution data set, synchrotron powder diffraction data of Eu(Cu,Al)$_{13-x}$ were obtained using the 11-BM beamline (λ = 0.412477 Å) at the Advanced Photon Source within Argonne National Laboratory (ANL).[31] The data points were collected over a 2θ span of 0.5°−47.5° with a step size of 0.001° and step time of 0.1 s. Rietveld refinement was employed to optimize the structure models of Eu(Cu,Al)$_{13-x}$ using the GSAS and EXPGUI packages.[32,33] Details regarding the data collection and the models yielded from the Rietveld refinements are given Table 4. The atomic positions with site occupancies and isotropic atomic displacement parameters are provided in Table 5.

Physical Properties Measurements. Magnetization data for all compounds were collected using a 9-T Quantum Design Physical Property Measurement System (PPMS). The temperature-dependent magnetization was obtained under zero-field cooled (ZFC) conditions from 3 to 300 K with an applied field of 0.1 T for the Pr(Cu,Al,Ga)$_{13-x}$, Eu(Cu,Al,Ga)$_{13-x}$, and Eu(Cu,Al)$_{13-x}$ analogues

Table 4. Crystallographic Parameters for Eu(Cu,Al)$_{13-x}$ Obtained from Rietveld Refinement

	Model 1	Model 2
composition	$EuCu_{6.78}Al_{6.22}$	$EuCu_{6.87}Al_{5.98}$
space group	$Fm\bar{3}c$	
a (Å)	11.932280(9)	
V (Å^3)	1698.910(4)	
Z	8	
temperature (K)	ambient	
[a] R_p	0.0506	
[b] R_{wp}	0.0687	
[c] R_{exp}	0.0480	
[d] χ	1.43	

[a] $R_p = \sum\|Y_o - Y_c\| / \sum Y_o$. [b] $R_{wp} = [M/\sum w(Y_o^2)]^{1/2}$. [c] $R_{exp} = R_{wp}/(\chi^2)^{1/2}$. [d] $\chi = (M/N_{obs} - N_{va})^{1/2}$.

dx.doi.org/10.1021/ic301024t | Inorg. Chem. 2012, 51, 10193−10202

Table 5. Atomic Fractional Coordinates, Site Occupancies, and U_{iso} for $Eu(Cu,Al)_{13-x}$ Obtained from Rietveld Refinement

atom	Wyckoff Site	x	y	z	occupancy	U_{iso} (Å^2)
			Model 1			
Eu1	8*a*	$^1/_4$	$^1/_4$	$^1/_4$	1	0.00793(4)
Cu1 (M1)	8*b*	0	0	0	0.7654(21)	0.00922(12)
Al2 (M1)	8*b*	0	0	0	0.2346(21)	0.00922(12)
Cu2 (M2)	96*i*	0.117235(15)	0.177245(15)	0	0.5015(9)	0.01078(5)
Al2 (M2)	96*i*	0.117235(15)	0.177245(15)	0	0.4985(9)	0.01078(5)
			Model 2			
Eu1	8*a*	$^1/_4$	$^1/_4$	$^1/_4$	1	0.00794(4)
Cu1 (M1)	8*b*	0	0	0	0.8587(13)	0.00915(12)
Cu2 (M2)	96*i*	0.117230(15)	0.177238(15)	0	0.5013(9)	0.01077(5)
Al2 (M2)	96*i*	0.117230(15)	0.177238(15)	0	0.4987(9)	0.01077(5)

and 1 T for $Ce(Cu,Al,Ga)_{13-x}$. Field-dependent measurements for $Ce(Cu,Al,Ga)_{13-x}$, $Pr(Cu,Al,Ga)_{13-x}$, and $Eu(Cu,Al,Ga)_{13-x}$ were performed at 3 K for fields ranging between 0 and 9 T. Additionally, field-dependent measurements for $Eu(Cu,Al,Ga)_{13-x}$ and $Eu(Cu,Al)_{13-x}$ were run at 2 K, 3 K, 5 K, 7 K, 9 K, 11 K, 15 K, and 20 K for fields between 0 and 5 T, and at 3 K, 5 K, 10 K, 15 K, 20 K, and 25 K for fields between 0 and 5 T, respectively. The temperature-dependent electrical resistivity (3 to 300 K) for $Ln(Cu,Al,Ga)_{13-x}$ (*Ln* = La−Pr and Eu) was measured using a standard four-probe ac-procedure with the PPMS. Pt wires with a diameter of 1 mil were mounted onto these samples with silver epoxy. Heat capacity measurements of $Ln(Cu,Al,Ga)_{13-x}$ (*Ln* = La−Pr and Eu) were also performed between 2 K−60 K.

RESULTS AND DISCUSSION

Structure Refinement. $Ln(Cu,Al,Ga)_{13-x}$ (*Ln* = La−Pr and Eu) adopts the well-known $NaZn_{13}$ structure-type which crystallizes in the cubic $Fm\bar{3}c$ space group with the *Ln*, M1, and M2 occupying the 8*a*, 8*b*, and 96*i* Wyckoff sites, respectively. Figure 1 shows the M1-centered M2 icosahedra with the La atoms occupying the cavities between the icosahedra. As the difference between the Cu and Ga X-ray form factors are small, attempts to freely model the Cu, Al, and Ga disorder without using a large number of constraints and restraints on the 8*b* and 96*i* positions were unsuccessful. These positions could be modeled with mixed occupancies containing just Cu and Al, similar to the modeling strategy employed for $EuCu_{6.5}Al_{6.5}$.[23] Although the differences in the neutron scattering lengths for Cu and Ga are fairly small 7.718(4) fm and 7.288(2) fm,[34] respectively, it was nevertheless expected that the contrast between the Cu and Ga neutron scattering lengths would overcome the problems experienced in modeling the Cu/Ga disorder via XRD. However, we found that the variation in scattering lengths (b_c^2 ratio of Cu and Ga = 1.12) was not significant enough to freely refine the mixed occupancy sites in the structures. A recently published neutron study of $Ba_8(Al,Si)_{46}$ clathrates also experienced this difficulty with a b_c^2 ratio of Si/Al = 1.45.[35] Therefore, our diffraction models required the use of linear free variable restraints (SHELXL's SUMP command) with the EDS results as target values. Because of the similarities in the crystal structure and refinement results of the synthesized series, the detailed discussion of the neutron models is limited to the lanthanum analogue.

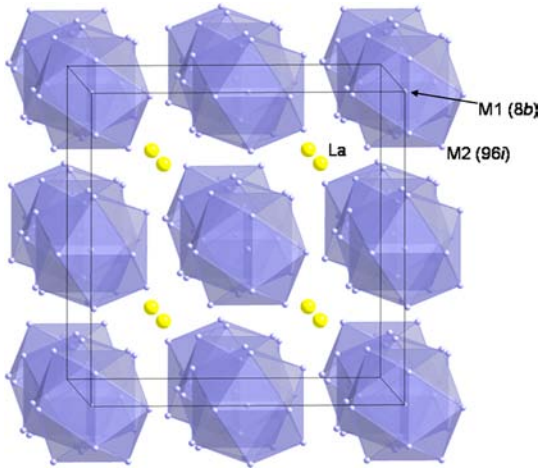

Figure 1. Crystal structure of $La(Cu,Al,Ga)_{13-x}$ is depicted where the M1-centered M2 icosahedral environment is emphasized. The yellow spheres represent La atoms.

The first model (please see Model 1 in Table 6) of the single-crystal neutron diffraction data for $La(Cu,Al,Ga)_{13-x}$ considered was based on the single crystal XRD models with full occupancy and Cu/Al mixing on both the 8*b* and 96*i* sites. While this model does not attempt to model gallium, the final refinement statistics indicate that it is a good fit to the observed data (R_1 = 0.057, wR_2 = 0.156, GOF = 1.08). The refined composition is $LaCu_{7.95}Al_{5.05}$, and the copper occupancy on the 8*b* and 96*i* sites is 68.9(19) % and 60.6(12) %, respectively. Analysis of a similar model (please see Model 2 in Table 6) with Ga substituted for Cu gives nearly identical statistics and slightly more gallium on each of the two sites 77(2) % (8*b*) and 67.4(13) % (96*i*).

A number of ways to model the Cu, Al, and Ga occupancies can be envisioned, and a model that initially yielded respectable refinement statistics took into account the mixing of Cu, Al, and Ga on both the 8*b* and 96*i* sites (please see Model 3 in Table 6). However, this model employs a large number of constraint parameters. The copper concentration and the total amount of Al, Cu, and Ga atoms in the asymmetric unit were restrained to EDS values of 6.3 and 12.6, respectively, using the SUMP command in SHELXL. The occupancies of Cu, Al, and Ga on each of the two sites were then refined using 1/3 as the initial free variables for the occupancies. This model yields compositional results comparable to the EDS composition and yields similar refinement statistics (R_1 = 0.056, wR_2 = 0.153, GOF = 1.05) compared to Models 1 and 2. However, analysis of the initial conditions (elemental occupancy values) indicated that the refinement was susceptible to a number of local minima, many of which were unrealistic (site occupancies larger than 100% or less than 0% without additional restraints). Additionally, the data were modeled by taking into account

dx.doi.org/10.1021/ic301024t | Inorg. Chem. 2012, 51, 10193−10202

Table 6. Summary of the Neutron Models for $La(Cu,Al,Ga)_{13-x}$

	$La(Cu,Al,Ga)_{13-x}$	$La(Cu,Al,Ga)_{13-x}$	$La(Cu,Al,Ga)_{13-x}$	$La(Cu,Al,Ga)_{13-x}$
	Model 1	Model 2	Model 3	Model 4
refined formula	$LaCu_{7.95}Al_{5.05}$	$LaGa_{8.85}Al_{4.15}$	$LaCu_{6.33}Ga_{2.12}Al_{4.17}$	$LaCu_{6.33}Ga_{1.97}Al_{4.53}$
space group	$Fm\bar{3}c$	$Fm\bar{3}c$	$Fm\bar{3}c$	$Fm\bar{3}c$
crystal system	cubic	cubic	cubic	cubic
a (Å)	11.897(4)	11.897(4)	11.897(4)	11.897(4)
V (Å^3)	1683.7(10)	1683.7(10)	1683.7(10)	1683.7(10)
Z	8	8	8	8
S	1.08	1.08	1.05	1.08
$R_1[F^2 > 2\sigma(F^2)]^a$	0.057	0.057	0.056	0.057
$wR_2(F^2)^b$	0.156	0.156	0.153	0.156
$\Delta\rho_{max}$ (fm Å^{-3})	1.60	1.60	1.76	1.60
$\Delta\rho_{min}$ (fm Å^{-3})	−1.30	−1.30	−1.30	−1.30

$^a R_1(F) = \sum||F_o| - |F_c||/\sum|F_o|$. $^b wR_2(F^2) = \{\sum[w(F_o^2 - F_c^2)^2]/\sum[w(F_o^2)^2]\}^{1/2}$.

mixing of Cu/Al or Cu/Ga on the 8*b* site, while at the same time mixing Cu, Al, and Ga on 96*i* site. Similar to the model just described, these models gave unrealistic results (site occupancies larger than 100% or less than 0% without additional restraints) depending on the initial parameters used for the occupancy of Cu/Al and Cu/Ga of the 8*b* site.

A literature study revealed a more intricate picture. A number of AM_xT_{13-x} (A = Ba, Sr, La, Eu; M = Cu, Ag; T = Al, Ga, In) compounds showed that the trielide and the transition metal mix on both the 8*b* and 96*i* sites.[23] However, the 8*b* site of the copper analogues was preferentially occupied by copper atoms (91% in $BaCu_5Al_8$ and 72% in $EuCu_{6.5}Al_{6.5}$). Furthermore, a recent reinvestigation of $EuZn_{13-x}$ shows that this structurally related phase is not fully stoichiometric, and the true composition is approximately $EuZn_{12.75}$. The Zn at the center of the icosahedron (8*b*) is partially occupied, whereas the Zn atoms (96*i*) at the corners of the icosahedron are fully occupied.[36] It was concluded that the partial occupancy helps the material reach the optimal number of valence electrons as discussed in detail by Nordell and Miller.[23]

Taking into consideration the results of these two studies reported for the site occupancy of the analogous compounds led us to a model where Cu alone (partially) occupied the 8*b* site, while the 96*i* site is fully occupied with Al, Cu, and Ga substitutionally disordered on this site (please see Model 4 in Table 6). We note that a similar approach was effective in modeling the disorder of $Ln(Cu,Ga)_{13-x}$, where Cu partially occupied the 8b site and Cu/Ga were mixed on the 96*i* site.[16] Similar to the model discussed previously, only the overall Cu composition distributed over both sites was restrained to the EDS value. The composition for $La(Cu,Al,Ga)_{13-x}$ resulting from this refinement (R_1 = 0.057, wR_2 = 0.156, GOF = 1.08) is in excellent agreement with the EDS composition (refined formula of $LaCu_{6.33}Al_{4.53}Ga_{1.97}$ compared to normalized EDS formula of $LaCu_{6.3(6)}Al_{4.2(8)}Ga_{2.1(1)}$). The refined composition in Table 1 of Ce also matches the EDS values well, while the refined compositions of the Pr and Eu analogues are not as aluminum rich compared to the EDS results. In addition, this model is impervious to the local minimum problem as described above. One final result that lends credence to this particular model is that the M2 (96*i*) atomic displacement parameters (ADPs) are slightly elongated, and the long axis (U^{11}) points toward the center of the icosahedron that limits the partial occupancy of the copper atom at the center of the icosahedron (8*b*) allowing the atoms of the icosahedral framework to relax inward, also observed in $EuZn_{12.75}$.[36]

Additionally, X-ray models have been generated where the compositions obtained from the final neutron models for each analogue were applied and used as restraints. Results from these models are presented in Supporting Information, Table S4 and fit well to the observed X-ray data.

Two models were found suitable to describe the structure of $Eu(Cu,Al)_{13-x}$, and we found minimal differences with the number of parameters used and identical final statistics. The two models differ in the way the disorder is refined on the 8*b* Wyckoff position. In the first model (Model 1) Cu and Al were modeled as occupational disordered on the 8*b* site, while the second model (Model 2) considers only Cu statistically disordered on the 8*b* Wyckoff site. The results of the Rietveld refinements are shown in Figure 2 (only a small portion of the collected data are shown for clarity), the compositions, lattice parameters and refinement statistics are provided in Table 4, and the atomic coordinates, site occupancies, and displacement parameters are listed in Table 5. We do note, however, that a few small impurity peaks were observed in the diffraction pattern at $2\theta \sim 11.5°$; however, the highest intensity of these peaks was only approximately 600 counts above the background. The phase purity of this phase was estimated to be greater than 95% by comparing the ratio of the most intense impurity reflection (~ 600 counts) to the most intense peak of product phase (~ 80000 counts).

The unit cell volumes of $Ln(Cu,Al,Ga)_{13-x}$ (*Ln* = La−Pr and Eu), $Ln(Cu,Ga)_{13-x}$ (*Ln* = La−Nd and Eu),[16] and $Ln(Cu,Al)_{13}$ (*Ln* = La−Sm and Eu)[19] are plotted as a function of *Ln* in Figure 3. Also plotted for comparison is the volume for $Eu(Cu,Al)_{13-x}$ as obtained from our Rietveld refinement. A deviation in the trend of the unit cell volumes is observed for the Eu analogues implying that the Eu compounds adopt a +2 oxidation state. This deviation is consistent with the magnetism for $Eu(Cu,Al,Ga)_{13-x}$ and $Eu(Cu,Al)_{13-x}$ (discussed below). Attempts to prepare the latter lanthanide analogues $Ln(Cu,Al,Ga)_{13-x}$ resulted in structures that adopted the $ThMn_{12}$ structure-type, thus, implying that $Eu(Cu,Al,Ga)_{13-x}$ is the end-member for the $Ln(Cu,Al,Ga)_{13}$ series.

Physical Properties. The temperature-dependent magnetic susceptibility data for $Ln(Cu,Al,Ga)_{13-x}$ (*Ln* = Ce and Pr) are shown in Figure 4a, and the $Eu(Cu,Al,Ga)_{13-x}$ data are shown in the inset of this figure. No long-range magnetic order is observed down to 3 K for $Ce(Cu,Al,Ga)_{13-x}$ or $Pr(Cu,Al,Ga)_{13-x}$. From the maximum in the $-(dM/dT)_H$ vs *T* curve, $Eu(Cu,Al,Ga)_{13-x}$ the lower limit of the ferromagnetic ordering temperature (T_C) is approximately 6 K. The magnetic

dx.doi.org/10.1021/ic301024t | Inorg. Chem. 2012, 51, 10193−10202

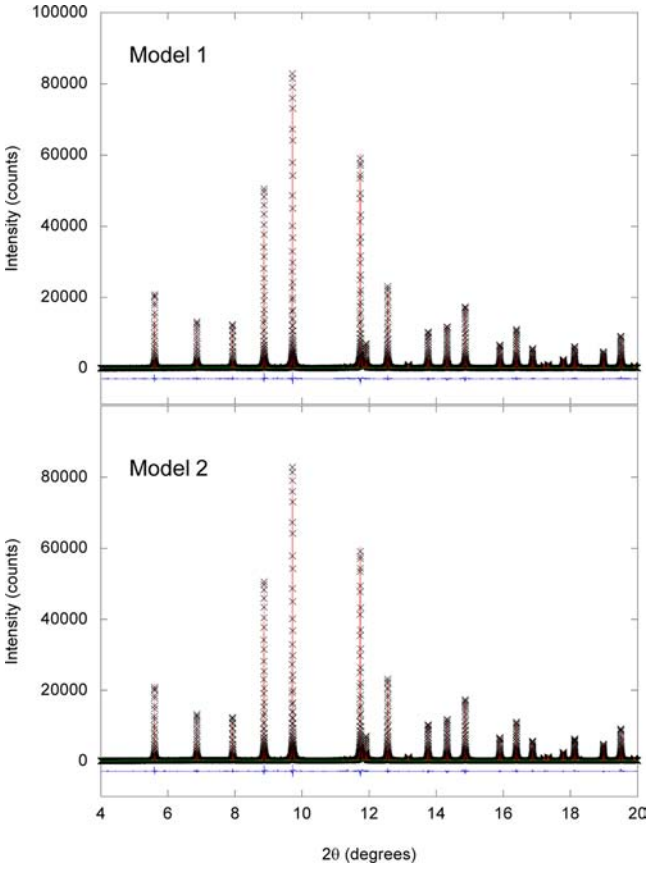

Figure 2. XRD powder pattern and Rietveld refinements of $Eu(Cu,Al)_{13-x}$ where two models have been considered. The black crosses, red fit line, green curve, and blue line correspond to the collected data, data fits, fitted background, and difference curve, respectively. Only a select 2θ range is shown for clarity.

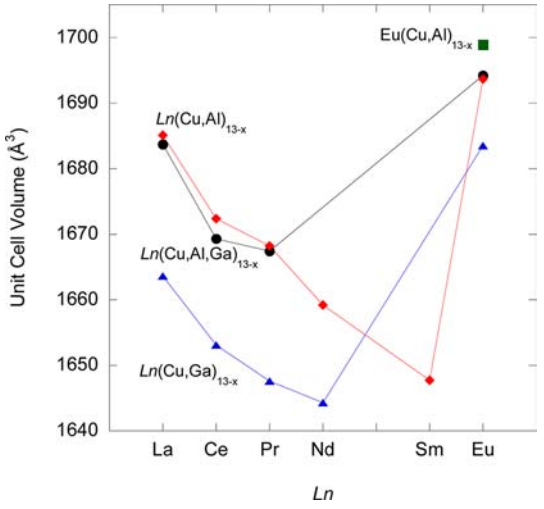

Figure 3. Unit cell volume vs lanthanide for $Ln(Cu,Al,Ga)_{13-x}$, $Ln(Cu,Ga)_{13-x}$,[16] $Ln(Cu,Al)_{13}$,[19] and $Eu(Cu,Al)_{13-x}$. The lines are used to guide the eyes.

susceptibility data for all analogues were fit using the Curie–Weiss equation, $\chi(T) = \chi_0 + C/(T - \theta)$, where χ_0 represents the temperature-independent contribution to the susceptibility which can be attributed to Pauli paramagnetism and/or Larmor diamagnetism, C is the Curie constant, and θ is the Weiss temperature. The effective moments for each analogue obtained from these fits are 2.26(4) μ_B for $Ce(Cu,Al,Ga)_{13-x}$, 3.43(9) μ_B for $Pr(Cu,Al,Ga)_{13-x}$, and 7.88(7) μ_B for $Eu(Cu,Al,Ga)_{13-x}$. These effective moments are in good agreement but are slightly smaller compared to the calculated values for Ce^{3+} (2.54 μ_B), Pr^{3+} (3.58 μ_B), and Eu^{2+} (7.94 μ_B), suggesting the local moment magnetism in these materials is due solely to the lanthanides. The results for each fit are summarized in Table 7. Figure 3 supports the notion that the Eu ions in $Eu(Cu,Al,Ga)_{13-x}$ are present in a divalent state. The Weiss temperatures extrapolated for $Ln(Cu,Al,Ga)_{13-x}$ (Ln = Ce and Pr) and $Eu(Cu,Al,Ga)_{13-x}$ are suggestive of weak antiferromagnetic and ferromagnetic correlations, respectively.

The field-dependent isothermal magnetization curves at 3 K for $Ln(Cu,Al,Ga)_{13-x}$ (Ln = Ce and Pr) are shown Figure 4b. The magnetization curves for both analogues exhibit the expected Brillouin behavior. Knowing that the ferromagnetic material $La(Fe,Si)_{13}$ crystallizes in the $NaZn_{13}$ structure-type and exhibits a giant magnetocaloric effect (MCE) near room temperature,[37,38] it was of interest to probe the magnetocaloric properties of $Eu(Cu,Al,Ga)_{13-x}$. Furthermore, $Eu(Cu,Al)_{13-x}$ was reported to order ferromagnetically at 16 K.[39] This compound was prepared and structurally characterized (Figure 2 and Tables 4 and 5) to compare its magnetocaloric properties to that of $Eu(Cu,Al,Ga)_{13-x}$. Our magnetic susceptibility data for $Eu(Cu,Al)_{13-x}$, shown in Figure 5, indicate that the lower limit of ferromagnetic order occurs around 8 K. Again, the maximum value in the $-(dM/dT)_H$ corresponds to the lower limit of T_C. Figure 6a and 6b show a series of magnetic isotherms for $Eu(Cu,Al,Ga)_{13-x}$ and $Eu(Cu,Al)_{13-x}$, respectively. The change in magnetic entropy, a measure of a material's MCE, can be estimated from a series of magnetic isotherms using the Maxwell relation, $\Delta S_{mag} = \sum_i (M_{i+1} - M_i)/(T_{i+1} - T_i)\cdot\Delta H_i$.[40−42] The magnetic entropy change as a function of temperature at ΔH = 2 T and ΔH = 5 T for both $Eu(Cu,Al,Ga)_{13-x}$ and $Eu(Cu,Al)_{13-x}$ is shown in Figure 7. The ΔS_{mag} for $Eu(Cu,Al,Ga)_{13-x}$ peaks around −11.5 J kg^{-1} K^{-1} near its T_C under an applied magnetic field change of 5 T, and the ΔS_{mag} for $Eu(Cu,Al)_{13-x}$ peaks around −10.5 J kg^{-1} K^{-1} near its T_C under an applied magnetic field change of 5 T. These values are smaller than that previously reported for the ferromagnets $ErNi_2$ (ΔS_{mag} = −24 J kg^{-1} K^{-1}, T_C = 6.6 K)[43] and $ErAl_2$ (ΔS_{mag} = −34 J kg^{-1} K^{-1}, T_C = 11.7 K)[44] under the same field conditions. The smaller ΔS_{mag} values for $Eu(Cu,Al,Ga)_{13-x}$ and $Eu(Cu,Al)_{13-x}$ are consistent with the Ln being surrounded by a more magnetically dilute matrix compared to $ErNi_2$ and $ErAl_2$.

The normalized resistance as a function of temperature is shown in Figure 8 for $Ln(Cu,Al,Ga)_{13-x}$ (Ln = La, Ce, Pr, and Eu). All analogues display metallic behavior. The ferromagnetic ordering in $Eu(Cu,Al,Ga)_{13-x}$ is evident in the inset of Figure 8, where a sharp decrease in the resistivity occurs near the Curie temperature, indicating a decrease in the spin-disorder scattering.

The specific heat capacities C_p of $Ln(Cu,Al,Ga)_{13-x}$ (Ln = La–Pr and Eu) are shown in Figure 9. The heat capacities for the Ce and Eu analogues deviate from the nonmagnetic La analogue at low temperatures, while this deviation for the Pr analogue can be seen at a much higher temperature, $T \sim 30$ K. This indicates that the magnitude of the magnetic entropy ΔS_{mag} is large for $Pr(Cu,Al,Ga)_{13-x}$. The thermodynamic evidence for the ferromagnetic ordering in $Eu(Cu,Al,Ga)_{13-x}$ is observed as a large peak in the specific heat below ~5 K which peaks at the Curie temperature. This deviation in the C_p

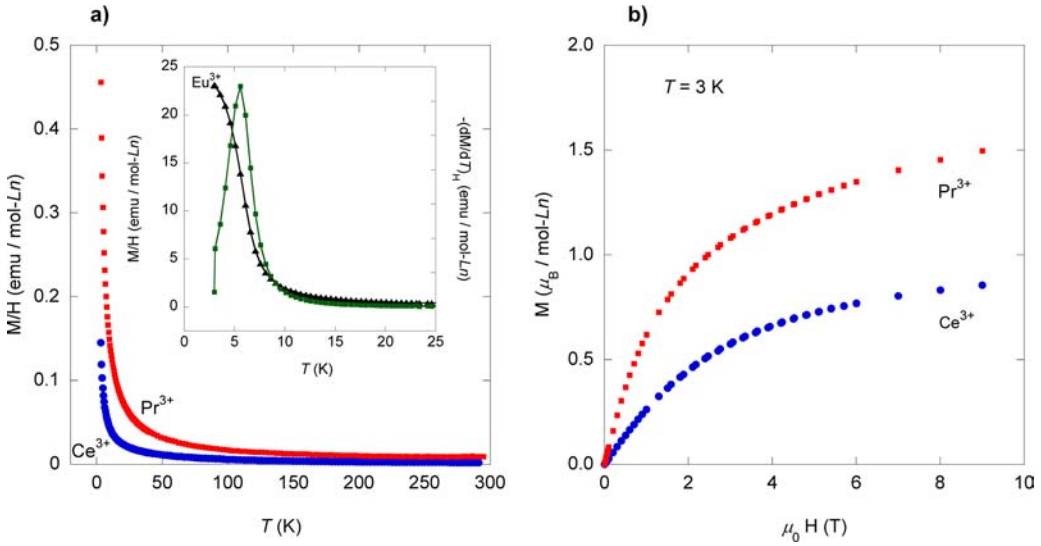

Figure 4. (a) Magnetic susceptibility of $Ln(Cu,Al,Ga)_{13-x}$ (Ln = Ce and Pr). The inset shows the magnetic susceptibility and $-(dM/dT)_H$ vs T curve for $Eu(Cu,Al,Ga)_{13-x}$. (b) Field-dependent isothermal magnetization at 3 K for $Ln(Cu,Al,Ga)_{13-x}$ (Ln = Ce and Pr).

Table 7. Magnetic Properties of $Ln(Cu,Al,Ga)_{13-x}$ (Ln = Ce, Pr, and Eu)

	$Ce(Cu,Al,Ga)_{13-x}$	$Pr(Cu,Al,Ga)_{13-x}$	$Eu(Cu,Al,Ga)_{13-x}$
field (H) Oe	1 T	0.1 T	0.1 T
fit region (K)	80−255	15−115	31−287
χ_0 (emu/mol-Ln)	−0.00015(4)	0.00268(7)	0.0051(4)
C (cm^3 K/mol)	0.64(1)	1.47(4)	7.77(7)
θ (K)	−3(1)	−0.52(4)	4.0(2)
μ_{calc} (μ_B)	2.54	3.58	7.94
μ_{eff} (μ_B)	2.26(4)	3.43(9)	7.88(7)

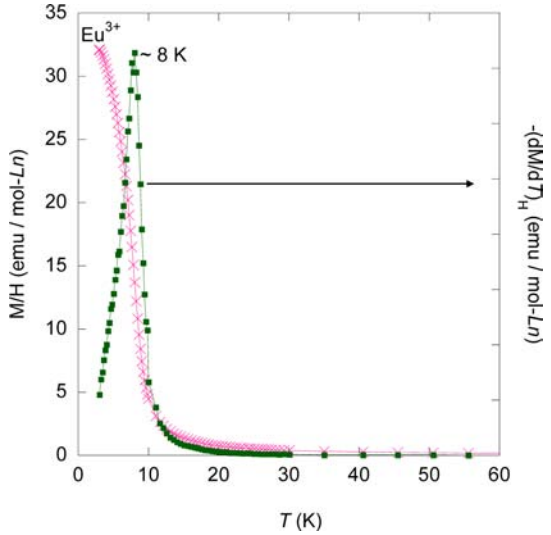

Figure 5. Magnetic susceptibility of $Eu(Cu,Al)_{13-x}$ (left) and the corresponding $-(dM/dT)_H$ vs T curve (right).

for $Eu(Cu,Al,Ga)_{13-x}$ coincides with the magnetic phase transition observed in the magnetic susceptibility (Figure 4a inset). Figure 9b shows the specific heat capacity divided by temperature C_p/T versus T^2 for all analogues. The magnetic phase transition for $Eu(Cu,Al,Ga)_{13-x}$ can be seen more clearly in this figure. Additionally, upturns in the C_p/T vs T^2 curves for both $Ce(Cu,Al,Ga)_{13-x}$ and $Pr(Cu,Al,Ga)_{13-x}$ are observed at low temperature. This suggests possible transitions just below the lowest temperature for these measurements, or the proximity to nuclear Schottky peaks usually observed at very low temperatures.

Fits of the standard form, $C_p/T = \gamma + \beta T^2$, to our C_p/T vs T^2 data for $Ln(Cu,Al,Ga)_{13-x}$ (Ln = La−Pr and Eu) were performed to determine the Sommerfeld coefficients (γ) for each analogue. The best fit values for γ determined from this fitting procedure are 1.65 mJ/mol-K^2, 40.8 mJ/mol-K^2, 356 mJ/mol-K^2, and 7.08 mJ/mol-K^2 for $La(Cu,Al,Ga)_{13-x}$, $Ce(Cu,Al,Ga)_{13-x}$, $Pr(Cu,Al,Ga)_{13-x}$, and $Eu(Cu,Al,Ga)_{13-x}$, respectively. The fit regions for each analogue are shown in Figure 9b, and the temperature regions to which each fit was performed were approximately 3−12 K, 9−21 K, 25−32 K, and 14−20 K for $La(Cu,Al,Ga)_{13-x}$, $Ce(Cu,Al,Ga)_{13-x}$, $Pr(Cu,Al,Ga)_{13-x}$, and $Eu(Cu,Al,Ga)_{13-x}$, respectively. The value of γ for $Pr(Cu,Al,Ga)_{13-x}$ obtained by our fitting procedure is significantly larger than that found in simple metals such as Cu ($\gamma \sim 1$ mJ/mol-K^2). The large Sommerfeld coefficient determined for $Pr(Cu,Al,Ga)_{13-x}$ may be indicative of the formation of an enhanced electron mass state at low temperatures.[3,45−48]

The magnetic contribution to the specific heat capacity C_{mag} for $Ln(Cu,Al,Ga)_{13-x}$ (Ln = Ce, Pr, and Eu) was estimated as the difference in the specific heats of $Ln(Cu,Al,Ga)_{13-x}$ (Ln = Ce, Pr, and Eu) and the nonmagnetic analogue, $La(Cu,Al,Ga)_{13-x}$, where it was assumed that the lattice contribution for each analogue was approximately equal to the specific heat of $La(Cu,Al,Ga)_{13-x}$. The magnetic entropy S_{mag} for $Ln(Cu,Al,Ga)_{13-x}$ (Ln = Ce, Pr, and Eu) was determined by integrating the magnetic heat capacity divided by temperature C_{mag}/T and is shown in the inset of Figure 9b. The magnetic entropy curves for $Ce(Cu,Al,Ga)_{13-x}$ and $Eu(Cu,Al,Ga)_{13-x}$ never approach the expected entropy values of $R \ln(2S + 1)$, where $S = 1/2$ and $S = 7/2$ for the Ce and Eu analogues, respectively. This may be attributed to the lowest temperature measurements of the heat capacity, only going down to ~2 K, where additional magnetic entropy for $Ce(Cu,Al,Ga)_{13-x}$ and $Eu(Cu,Al,Ga)_{13-x}$ could be integrated. The magnetic entropy recovered for $Pr(Cu,Al,Ga)_{13-x}$ exceeds

dx.doi.org/10.1021/ic301024t | Inorg. Chem. 2012, 51, 10193−10202

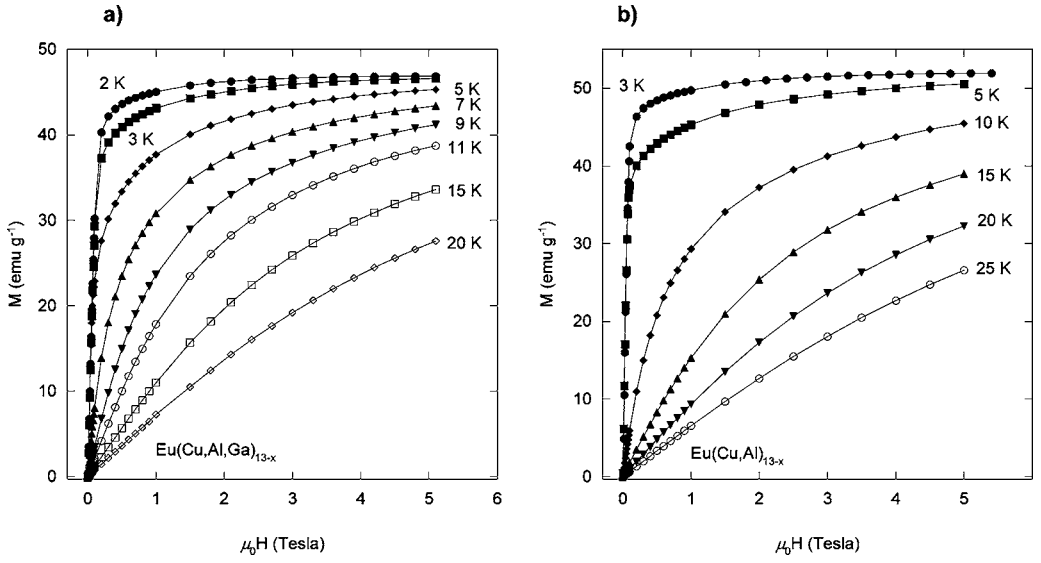

Figure 6. Magnetic isotherms versus field for (a) $Eu(Cu,Al,Ga)_{13-x}$ and (b) $Eu(Cu,Al)_{13-x}$.

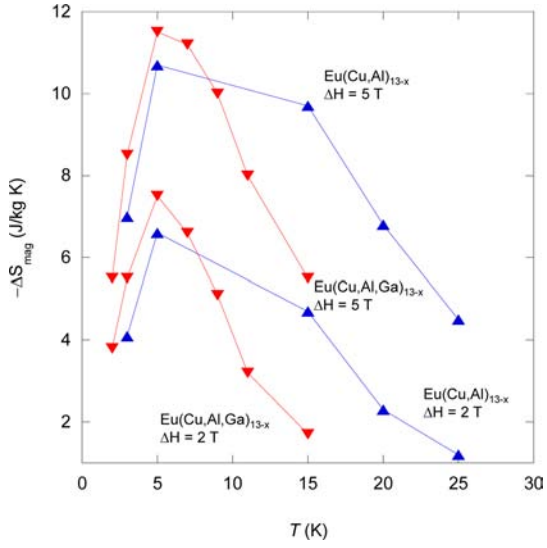

Figure 7. $-\Delta S_{mag}$ as a function of temperature for $Eu(Cu,Al,Ga)_{13-x}$ (red) and $Eu(Cu,Al)_{13-x}$ (blue) under the applied field changes (ΔH) of 2 and 5 T.

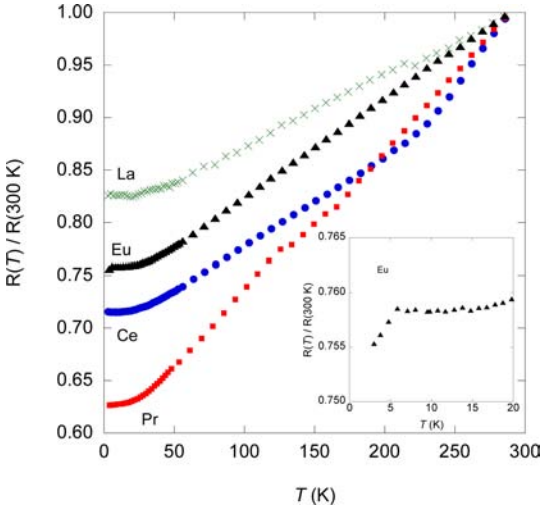

Figure 8. Temperature-dependent normalized resistance of $Ln(Cu,Al,Ga)_{13-x}$ (Ln = La, Ce, Pr, and Eu).

the expected entropy of $R\ln(2S + 1)$ where $S = 1$, but begins to saturate below $R\ln(2J + 1)$ where $J = 4$.

The origin of heavy-fermion behavior in Pr-based compounds is thought to be one to two mechanisms: either (1) the quadrupolar Kondo effect[14] or (2) the excitonic mass enhancement[49] associated with low energy split crystal electric field (CEF) levels. The latter mechanism was proposed by Fulde and Jensen to account for the low temperature mass enhancement of Pr metal.[50] Here the conduction electrons inelastically scatter from the low lying excited CEF levels of the 4f electrons which results in their enhanced mass. These mechanisms differ from the traditional mechanism leading to the formation of heavy quasi-particles in Ce, Yb, and U compounds, where the heavy-fermion behavior is due to the complete compensation of the magnetic moments of the lanthanide ions by the conduction electrons via the formation of a Kondo coherent state at low temperatures.[14,51]

The observed physical properties of $Pr(Cu,Al,Ga)_{13-x}$ bear a striking resemblance to the physical properties of other Pr-based heavy-fermion compounds, where the heavy mass state is thought to arise from the excitonic mass enhancement mechanism.[14,51−54] The Sommerfeld coefficient determined for $Pr(Cu,Al,Ga)_{13-x}$ (356 mJ/mol-K^2) is comparable to, and in some cases larger, than the Sommerfeld coefficients of other Pr intermetallics, such as $PrOs_4Sb_{12}$ (350 mJ/mol-K^2),[51] $Pr_2Rh_3Ge_5$ (80 mJ/mol-K^2),[52] $PrIr_2B_2C$ (300 mJ/mol-K^2),[53] and $PrRh_2B_2C$ (300 mJ/mol-K^2).[54] Additionally, the magnetic entropy of $Pr(Cu,Al,Ga)_{13-x}$ exceeds $R\ln(3)$ above 20 K (Figure 9b). Similar behavior was observed for the heavy-fermion compounds $Pr_2Rh_3Ge_5$,[52] $PrIr_2B_2C$,[53] and $PrRh_2B_2C$,[54] where the authors claimed that the increased values of the magnetic entropy above $R\ln(3)$ were due to the electronic excitations of low lying CEF levels. A better understanding of the CEF levels of $Pr(Cu,Al,Ga)_{13-x}$ is needed to clarify the underlying physics which leads to the enhanced Sommerfeld coefficient. Further studies, such as inelastic neutron scattering experiments would be useful for determining the energy

dx.doi.org/10.1021/ic301024t | Inorg. Chem. 2012, 51, 10193−10202

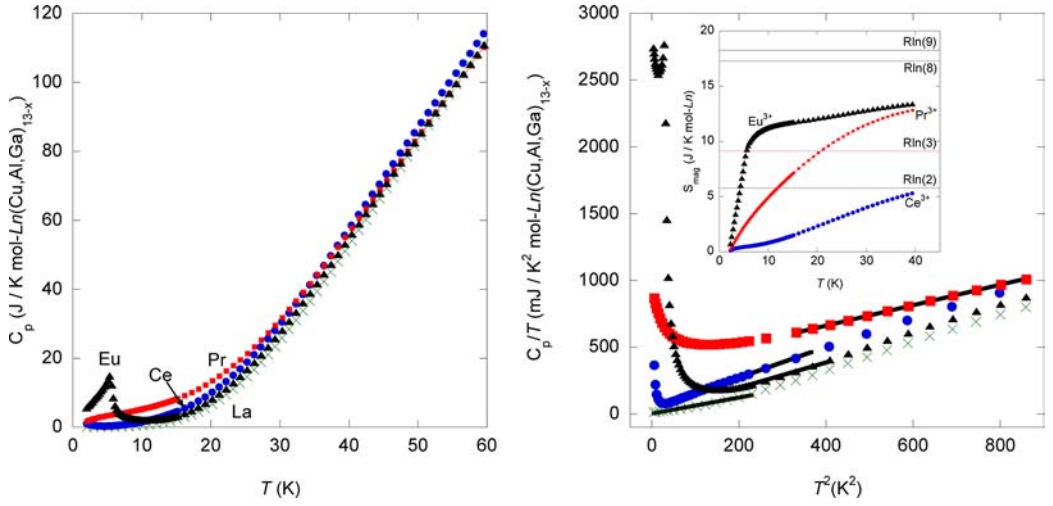

Figure 9. (a) Specific heat capacities C_p of $Ln(Cu,Al,Ga)_{13-x}$ (Ln = La−Pr and Eu) as a function of temperature. (b) The specific heat capacity divided by temperature C_p/T vs T^2. The inset shows the magnetic entropy S_{mag} as a function of temperature for $Ln(Cu,Al,Ga)_{13-x}$ (Ln = Ce, Pr, and Eu).

differences between the excited CEF levels of $Pr(Cu,Al,Ga)_{13-x}$, as well as understanding its low temperature ground state.

CONCLUSIONS

Large single crystals of $Ln(Cu,Al,Ga)_{13-x}$ (Ln = La−Pr, and Eu) adequate for neutron diffraction were grown using an Al/Ga flux. XRD and neutron diffraction experiments were conducted using these single crystals to fully elucidate the disorder on the 8*b* and 96*i* Wyckoff sites. Because of the similarities of the Cu and Ga X-ray form factors and neutron scattering lengths, the Cu, Al, and Ga occupational disorder was difficult to definitively elucidate. Therefore, many models of the neutron data were investigated. The first set of models took into account only Cu/Al or Ga/Al mixing of the 8*b* and 96*i* Wyckoff sites. These individual models fit the neutron data well and yielded similar refinement statistics, and therefore, it was concluded that neutron scattering lengths of Cu and Ga were too similar and that restraints employing the elemental compositions from our EDS experiments would need to be used in subsequent refinements. All refinement models which attempted to mix combinations of Cu, Al, and/or Ga on the 8*b* Wyckoff site were prone to local minima and in some cases depending on the starting free variables yielded unrealistic solutions (site occupancies larger than 100% or less than 0%). Refinement of the models against the neutron data obtained for each analogue, which yield excellent statistics, were not prone to local minima, and reproduced the EDS compositions without a large number of restraints or parameters, considered an 8*b* Wyckoff site with only occupationally disordered Cu and substitutional disorder of Cu, Al, and Ga on the 96*i* Wyckoff site. This final model is very similar to the models reported for other compounds adopting the $NaZn_{13}$ structure-type as described by Bobev.[36] Additionally, an arc-melted button of $Eu(Cu,Al)_{13-x}$ was prepared to compare its magnetic properties to those of $Eu(Cu,Al)_{13-x}$. This button was annealed before it was cut, and the cut portions were used for X-ray powder diffraction and magnetic properties measurement. The X-ray powder diffraction data collected at the Advanced Photon Source within Argonne National Laboratory were modeled successfully using the Rietveld refinement technique as discussed above.[31]

The magnetic, transport, and thermodynamic properties of $Ln(Cu,Al,Ga)_{13-x}$ (Ln = La−Pr, and Eu) were investigated. All analogues display metallic behavior from 3 to 300 K. $Ce(Cu,Al,Ga)_{13-x}$ and $Pr(Cu,Al,Ga)_{13-x}$ displayed paramagnetic behavior over all temperatures measured in the magnetic susceptibility. $Eu(Cu,Al,Ga)_{13-x}$ orders ferromagnetically around 6 K. Since $La(Fe,Si)_{13}$ orders ferromagnetically, exhibits a giant magnetocaloric effect, and is isostructural to $Eu(Cu,Al,Ga)_{13}$, the magnetocaloric properties of $Eu(Cu,Al,Ga)_{13-x}$ were examined.[55] Additionally, the magnetocaloric properties of the ferromagnet $Eu(Cu,Al)_{13}$ ($T_c \sim 8$ K) were studied. The ΔS_{mag} values determined for $Eu(Cu,Al,Ga)_{13-x}$ and $Eu(Cu,Al)_{13-x}$ were found to be smaller than the ΔS_{mag} values for other magnetocaloric materials ($ErNi_2$ and $ErAl_2$) that order ferromagnetically in the same temperature region. This is consistent with the Ln being surrounded by a more magnetically dilute matrix compared to $ErNi_2$ and $ErAl_2$. Additionally, the Sommerfeld coefficient for $Pr(Cu,Al,Ga)_{13-x}$ was found to be large with $\gamma \sim 350$ mJ/mol-K^2. Similar to the heavy fermion compound $Pr(Cu,Ga)_{13-x}$[16] and other Pr based heavy fermion compounds, no Kondo features were observed in the resistivity of $Pr(Cu,Al,Ga)_{13-x}$. Therefore, the enhancement of the Sommerfeld coefficient for $Pr(Cu,Al,Ga)_{13}$ is likely not the result of the formation of a Kondo coherent state. Further studies at low temperatures are needed to determine the origin of the large Sommerfeld coefficient of $Pr(Cu,Al,Ga)_{13-x}$.

ASSOCIATED CONTENT

Supporting Information

Crystallographic data in CIF format. Further details are given in Tables S1−S4. This material is available free of charge via the Internet at http://pubs.acs.org.

AUTHOR INFORMATION

Corresponding Author

*E-mail: jchan@lsu.edu. Phone: (225) 578-2695. Fax: (225) 578-3458.

Notes

The authors declare no competing financial interest.

■ ACKNOWLEDGMENTS

J.Y.C. would like to acknowledge support for this research from the National Science Foundation (NSF) through DMR1063735. D.P.Y acknowledges support from the NSF under Grant DMR1005764. E.M. acknowledges support from the NSF under Grant DMR0847681. The neutron diffraction data were collected at the Oak Ridge National Laboratory's Spallation Neutron Source; supported by the Division of Scientific User Facilities, Office of Basic Energy Sciences, U.S. Department of Energy, under contract DE-AC05-00OR22725 with UT Battelle, LLC. W.A.P., M.J.K., and G.T.M. would like to acknowledge the EPSCoR Travel Fellowship for traveling assistance. Funding for the EPSCoR Travel Fellowship is provided by the Department of Energy, Office of Basic Energy Sciences, through the EPSCoR Grant DE-FG02-08ER46528 to the University of Tennessee. Use of the Advanced Photon Source at Argonne National Laboratory was supported by the U.S. Department of Energy, Office of Science, Office of Basic Energy Sciences, under Contract No. DE-AC02-06CH11357.

■ REFERENCES

(1) Stewart, G. R. *Rev. Mod. Phys.* **1984**, *56*, 755−787.
(2) Markiv, V. Y.; Shevchenko, I. P.; Belyavina, N. N.; Kuzmenko, P. P. *Dopov. Akad. Nauk. A* **1986**, *48*, 78−81.
(3) Fisk, Z.; Sarrao, J. L.; Smith, J. L.; Thompson, J. D. *Proc. Natl. Acad. Sci. U.S.A.* **1995**, *92*, 6663−6667.
(4) Suski, W. The $ThMn_{12}$-Type Compounds of Rare Earths and Actinides: Structure, Magnetic and Related Properties. In *Handbook on the Physics and Chemistry of Rare Earths*; Gschneidner, K. A. J., Lyring, L., Eds.; Elsevier: New York, 1996; Vol. *22*, pp 143−294.
(5) Thomas, E. L.; Millican, J. N.; Okudzeto, E. K.; Chan, J. Y. *Comments Inorg. Chem.* **2006**, *27*, 1−39.
(6) Phelan, W. A.; Menard, M. C.; Kangas, M. J.; McCandless, G. T.; Drake, B. L.; Chan, J. Y. *Chem. Mater.* **2012**, *24*, 409−420.
(7) Ott, H. R.; Rudigier, H.; Fisk, Z.; Smith, J. L. *Phys. Rev. Lett.* **1983**, *50*, 1595−1598.
(8) Smith, J. L.; Fisk, Z.; Willis, J. O.; Batlogg, B.; Ott, H. R. *J. Appl. Phys.* **1984**, *55*, 1996−2000.
(9) Maple, M. B.; Chen, J. W.; Lambert, S. E.; Fisk, Z.; Smith, J. L.; Ott, H. R.; Brooks, J. S.; Naughton, M. J. *Phys. Rev. Lett.* **1985**, *54*, 477−480.
(10) Cox, D. L. *Phys. Rev. Lett.* **1987**, *59*, 1240−1243.
(11) Kim, J. S.; Stewart, G. R. *Phys. Rev. B* **1995**, *51*, 16190−16193.
(12) Besnus, M. J.; Kappler, J. P.; Meyer, A. *Solid State Commun.* **1983**, *48*, 835−838.
(13) Wilson, Z. S.; Macaluso, R. T.; Bauer, E. D.; Smith, J. L.; Thompson, J. D.; Fisk, Z.; Stanley, G. G.; Chan, J. Y. *J. Am. Chem. Soc.* **2004**, *126*, 13926−13927.
(14) Yatskar, A.; Beyermann, W. P.; Movshovich, R.; Canfield, P. C. *Phys. Rev. Lett.* **1996**, *77*, 3637−3640.
(15) Kadowaki, K.; Woods, S. B. *Solid State Commun.* **1986**, *58*, 507−509.
(16) Cho, J. Y.; Thomas, E. L.; Nambu, Y.; Capan, C.; Karki, A. B.; Young, D. P.; Kuga, K.; Nakatsuji, S.; Chan, J. Y. *Chem. Mater.* **2009**, *21*, 3072−3078.
(17) Shimura, Y.; Sakakibara, T.; Cho, J. Y.; Chan, J. Y. *J. Phys. Conf. Ser.* **2011**, *273*, 012054.
(18) Drake, B. L.; Capan, C.; Cho, J. Y.; Nambu, Y.; Kuga, K.; Xiong, Y. M.; Karki, A. B.; Nakatsuji, S.; Adams, P. W.; Young, D. P.; Chan, J. Y. *J. Phys.: Condens. Matter* **2010**, *22*, 066001.
(19) Felner, I. *J. Less-Common Met.* **1980**, *72*, 241−249.
(20) Cordier, G.; Czech, E.; Ochmann, H.; Schäfer, H. *J. Less-Common Met.* **1984**, *99*, 173−185.
(21) Cordier, G.; Czech, E.; Schäfer, H. *J. Less-Common Met.* **1985**, *108*, 225−239.
(22) Cordier, G.; Czech, E.; Schäfer, H.; Woll, P. *J. Less-Common Met.* **1985**, *110*, 327−330.
(23) Nordell, K. J.; Miller, G. J. *Inorg. Chem.* **1999**, *38*, 579−590.
(24) Altomare, A.; Burla, M. C.; Camalli, M.; Cascarano, G. L.; Giacovazzo, C.; Guagliardi, A.; Moliterni, A. G. G.; Polidori, G.; Spagna, R. *J. Appl. Crystallogr.* **1999**, *32*, 115−119.
(25) Sheldrick, G. M. *Acta Crystallogr., A* **2008**, *64*, 112−122.
(26) Otwinowski, Z.; Minor, W. In *Methods in Enzymology*; Carter, C. W., Jr., Sweet, R. M., Eds.; Academic Press: New York, 1997; Vol. *276*, Macromolecular Crystallography, Part A, pp 307−326.
(27) Jogl, G.; Wang, X. P.; Mason, S. A.; Kovalevsky, A.; Mustyakimov, M.; Fisher, Z.; Hoffman, C.; Kratky, C.; Langan, P. *Acta. Crystallogr., Sect. D* **2011**, *67*, 584−591.
(28) Hoffman, C.; Wang, X. P.; Frost, M. *SNS TOPAZ Single-Crystal Diffractometer*; http://neutrons.ornl.gov/instruments/SNS/TOPAZ, (accessed February 2012).
(29) Zikovsky, J.; Peterson, P. F.; Wang, X. P.; Frost, M.; Hoffmann, C. *J. Appl. Crystallogr.* **2011**, *44*, 418−423.
(30) Schultz, A. J.; Srinivasan, K.; Teller, R. G.; Williams, J. M.; Lukehart, C. M. *J. Am. Chem. Soc.* **1984**, *106*, 999−1003.
(31) Wang, J.; Toby, B. H.; Lee, P. L.; Ribaud, L.; Antao, S. M.; Kurtz, C.; Ramanathan, M.; Von Dreele, R. B.; Beno, M. A. *Rev. Sci. Instrum.* **2008**, *79*, 085105.
(32) Larson, A. C.; Von Dreele, R. B. Los Alamos National Laboratory Report LAUR 86-748; Los Alamos National Laboratory: Los Alamos, NM, 1995−2004; pp 1−224.
(33) Toby, B. H. *J. Appl. Crystallogr.* **2001**, *34*, 210−213.
(34) Sear, V. F. *Neutron News.* **1992**, *3*, 26−37.
(35) Roudebush, J. H.; de la Cruz, C.; Chakoumakos, B. C.; Kauzlarich, S. M. *Inorg. Chem.* **2011**, *51*, 1805−1812.
(36) Saparov, B.; Bobev, S. *J. Alloys Compd.* **2008**, *463*, 119−123.
(37) Shen, B. G.; Sun, J. R.; Hu, F. X.; Zhang, H. W.; Cheng, Z. H. *Adv. Mater.* **2009**, *21*, 4545−4564.
(38) Han, M. K.; Miller, G. J. *Inorg. Chem.* **2008**, *47*, 515−528.
(39) Felner, I.; Nowik, I. *J. Phys. Chem. Solids* **1982**, *43*, 463−465.
(40) Gschneidner, K. A.; Pecharsky, V. K. *Annu. Rev. Mater. Sci.* **2000**, *30*, 387−429.
(41) Gutfleisch, O.; Willard, M. A.; Bruck, E.; Chen, C. H.; Sankar, S. G.; Liu, J. P. *Adv. Mater.* **2011**, *23*, 821−842.
(42) Pecharsky, V. K.; Gschneidner, K. A. *Int. J. Refrig.* **2006**, *29*, 1239−1249.
(43) Tomokiyo, A.; Yayama, H.; Wakabayyashi, H.; Kuzuhara, T.; Hashimoto, T.; Sahashi, M.; Inomata, K. *Adv. Cryog. Eng.* **1986**, *32*, 295−301.
(44) Hashimoto, T.; Matsumoto, K.; Kurihara, T.; Numazawa, T.; Tomokiyo, A.; Yayama, H.; Goto, T.; Todo, S.; Sahashi, M. *Adv. Cryog. Eng.* **1986**, *32*, 279−286.
(45) Fisk, Z. *Science* **2007**, *318*, 1559−1560.
(46) Fisk, Z.; Hess, D. W.; Pethick, C. J.; Pines, D.; Smith, J. L.; Thompson, J. D.; Willis, J. O. *Science* **1988**, *239*, 33−42.
(47) Fisk, Z.; Ott, H. R.; Rice, T. M.; Smith, J. L. *Nature* **1986**, *320*, 124−129.
(48) Fisk, Z.; Sarrao, J. L.; Thompson, J. D. *Curr. Opin. Solid State Mater. Sci.* **1996**, *1*, 42−46.
(49) Goremychkin, E. A.; Osborn, R.; Bauer, E. D.; Maple, M. B.; Frederick, N. A.; Yuhasz, W. M.; Woodward, F. M.; Lynn, J. W. *Phys. Rev. Lett.* **2004**, *93*, 157003.
(50) Fulde, P.; Jensen, J. *Phys. Rev. B* **1983**, *27*, 4085−4094.
(51) Bauer, E. D.; Frederick, N. A.; Ho, P. C.; Zapf, V. S.; Maple, M. B. *Phys. Rev. B* **2002**, *65*, 100506.
(52) Anand, V. K.; Hossain, Z.; Geibel, C. *Phys. Rev. B* **2008**, *77*, 184407.
(53) Anupam; Anand, V. K.; Hossain, Z.; Adroja, D. T.; Geibel, C. *J. Phys.: Condens. Matter* **2011**, *23*, 376001.
(54) Anand, V. K.; Hossain, Z.; Chen, G.; Nicklas, M.; Geibel, C. *Phys. Rev. B* **2009**, *79*, 113107.
(55) Jia, L.; Sun, J. R.; Shen, J.; Gao, B.; Zhao, T. Y.; Zhang, H. W.; Hu, F. X.; Shen, B. G. *J. Alloys Compd.* **2011**, *509*, 5804−5809.